Journal of Biomechanics 82 (2019) 299–306

Contents lists available at ScienceDirect

Journal of Biomechanics

journal homepage: www.elsevier.com/locate/jbiomech
www.JBiomech.com

Evaluating residual strain throughout the murine female reproductive system

Daniel J. Capone [a], Gabrielle L. Clark [a], Derek Bivona [a,b], Benard O. Ogola [c], Laurephile Desrosiers [d], Leise R. Knoepp [d], Sarah H. Lindsey [c], Kristin S. Miller [a]

[a] Department of Biomedical Engineering, Tulane University, 6823 St. Charles Ave, New Orleans, LA 70118, USA
[b] Department of Biomedical Engineering, University of Virginia, 415 Lane Road, Charlottesville, VA 22908, USA
[c] Department of Pharmacology, Tulane University School of Medicine, 1430 Tulane Avenue, New Orleans, LA 70112, USA
[d] Department of Female Pelvic Medicine & Reconstructive Surgery, University of Queensland, Ochsner Clinical School, 1514 Jefferson Highway, New Orleans, LA 70121, USA

ARTICLE INFO

Article history:
Accepted 1 November 2018

Keywords:
Pelvic floor
Vagina
Cervix
Opening angle
Women's reproductive health

ABSTRACT

Mounting evidence suggests that cells within soft tissues seek to maintain a preferred biomechanical state. Residual stress is defined as the stress that remains in a tissue when all external loads are removed and contributes to tissue mechanohomeostasis by decreasing the transmural gradient of wall stress. Current computational models of pelvic floor mechanics, however, often do not consider residual stress. Residual strain, a result of residual stress can be quantitatively measured through opening angle experiments. Therefore, the objective of this study is to quantify the regional variations in opening angles along the murine female reproductive system at estrus and diestrus, to quantify residual strain in the maintenance state of sexually mature females. Further, evidence suggests that hydrophilic glycosaminoglycan/proteoglycans are integral to cervical remodeling. Thus, variations in opening angles following hypo-osmotic loading are evaluated. Opening angle experiments were performed along the murine reproductive system in estrus ($n = 8$) and diestrus ($n = 8$) and placed in hypo-osmotic solution. Measurements of thickness and volume were also obtained for each group. Differences ($p < 0.05$) in opening angle were observed with respect to region and loading, however, differences with respect to estrous stage were not significant. Thickness values were significant ($p < 0.05$) with respect to region only. The effects of both estrous cycle and region resulted in significant differences ($p < 0.05$) in observed volume. The observed regional differences indicate variation in the stress-free state among the reproductive system which may have implications for future computational models to advance women's reproductive health.

1. Introduction

Computational models of the female reproductive system and its supporting structures have been developed to better describe and predict the mechanics of the pelvic floor in both healthy and diseased states c.f., (Liao et al., 2014; Yang et al., 2016; Myers et al., 2010; Abramowitch et al., 2009; Lien et al., 2004). To date, however, these models largely do not incorporate residual stress, an important mechanical characteristic of soft tissue. Residual stress is defined as the stress that remains in a tissue when no external loads are applied, and induces a residual strain that can be quantitatively measured through opening angle experiments (Chuong and Fung, 1986). These residual stresses and strains are thought to contribute to tissue mechanohomeostasis (Takamizawa and Hayashi, 1987; Chuong and Fung, 1986). This has been shown most prevalently in arteries in which ignoring the effect of residual stress results in the development of a transmural stress gradient through the wall (Takamizawa and Hayashi, 1987, 1988). When residual stress is considered in healthy arteries this gradient is eliminated and an equidistribution of stress is observed (Han and Fung, 1996; Cardamone et al., 2009; Taber and Humphrey, 2001). Conversely, when considering residual stress in arteries experiencing abnormally high stresses (such as hypertension), a non-linear stress profile throughout the thickness of the wall is observed (Chuong and Fung, 1986; Fung, 1991; Haghighipour et al., 2010, Taghizadeh et al., 2015). Hence, incorporating residual stress into computational models may provide a more accurate calculation of the mechanical state of the pelvic floor, thus providing a framework to determine potential

E-mail addresses: dcapone@tulane.edu (D.J. Capone), gclark2@tulane.edu (G.L. Clark), djb6ab@virginia.edu (D. Bivona), bogola@tulane.edu (B.O. Ogola), laurephile.desrosiers@ochsner.org (L. Desrosiers), lknoepp@ochsner.org (L.R. Knoepp), lindsey@tulane.edu (S.H. Lindsey), kmille11@tulane.edu (K.S. Miller)

https://doi.org/10.1016/j.jbiomech.2018.11.001
0021-9290/

mechanical mechanisms of tissue remodeling observed during the disease state of the tissue.

Female reproductive organs continuously undergo extracellular matrix (ECM) remodeling during normal processes such as the estrous cycle, pregnancy, postpartum healing, and aging/menopause (Rodriguez-Pinon et al., 2015; Perry et al., 2012). A murine model was chosen due to its microstructural similarities to human reproductive tissues and prevalent use in pelvic floor disorder research c.f., (Abramowitch et al., 2009; Mahendroo, 2012; Westervelt and Myers, 2017; Elovitz and Mrinalini, 2004). There is an abundance of mechanical test data on the murine reproductive system that can be further complemented by the incorporation of residual strain data c.f., (Rahn et al., 2008; Yoshida et al., 2014; Elovitz and Mrinalini, 2004; Barnum et al., 2017; Robison et al., 2017).

In addition to differences in the growth and remodeling state, it is understood that the constituent makeup of the female reproductive system varies significantly with region, which may result in a spatial variability of the stress-free state of the tissue. It has also been suggested that tissue osmosis-induced swelling is closely linked to the residual stress due to turnover of the water sequestering glycosaminoglycans (GAGs) that are inherent in the ECM of women's reproductive organs (Guo et al., 2007; Sorrentino et al., 2015a; Azeloglu et al., 2008). Therefore, the objective of this study is to quantify the effects of estrous cycle, spatial variation (beginning at the ovaries and moving distally to the vagina), and hypo-osmotic loading on residual strain by means of opening angle experiments.

2. Methods

Sexually mature (4–6 month old, n = 16) female C57BL6 mice (The Jackson Laboratory, Bar Harbor, ME, USA) were euthanized (n = 8 at estrus, n = 8 at diestrus) and their reproductive systems were excised and stored at −20 °C in this Tulane University Animal Care and Use Committee approved study. Mice were allowed to acclimate for one week after delivery before euthanasia and were housed under standard conditions (standard bedding, light/dark cycles). After the acclimation period, the estrus cycle of each mouse was monitored daily by visual inspection until the desired phase of the cycle was identified (Byers et al., 2012). Samples were bathed in Hank's Balanced Saline Solution (HBSS) at room temperature before testing. With the use of an Olympus SZX12 microscope (Olympus America, Inc., Melville, NY, USA), pairs of rings of approximately 0.5 mm in width were cut transversely at six different positions along the reproductive system (Fig. 1). These positions included the upper right and left uteri near the ovary (UOV), right and left mid-uterus (U), right and left uteri near the mid-cervix (UCER), mid-cervix (CER), external os/vaginal cervix (VCER), and the vagina (V) (Fig. 1). One ring from each of the pairs was randomly placed in 33% hypo-osmotic HBSS with 46 mM sodium chloride while the other ring remained in control HBSS with 134 mM sodium chloride (Sorrentino et al., 2015b). Following a 30 min equilibration, the rings were imaged with a Moticam 580 microscope camera (Motic, Inc., Richmond, British Columbia, Canada). Then the anterior section of each ring was cut radially, and the near-zero stress states were imaged 30 min later (Ferruzzi et al., 2013; Amin, 2012; Humphrey, 2002). Using the angle tool in ImageJ (ImageJ, U.S. National Institutes of Health, Bethesda, ME, USA), opening angles were measured from the midpoint of the inner wall to the tips of the inner wall of the open sections. Opening angles of the rings of the left and right upper uterus near the ovary, left and right mid-uterus, and left and right uteri near the mid-cervix were averaged at each of these locations.

2.1. Histology and immunohistochemistry

To examine histological (n = 3) and immunohistochemical (n = 3) changes with regional location, U, UCER, VCER, and V

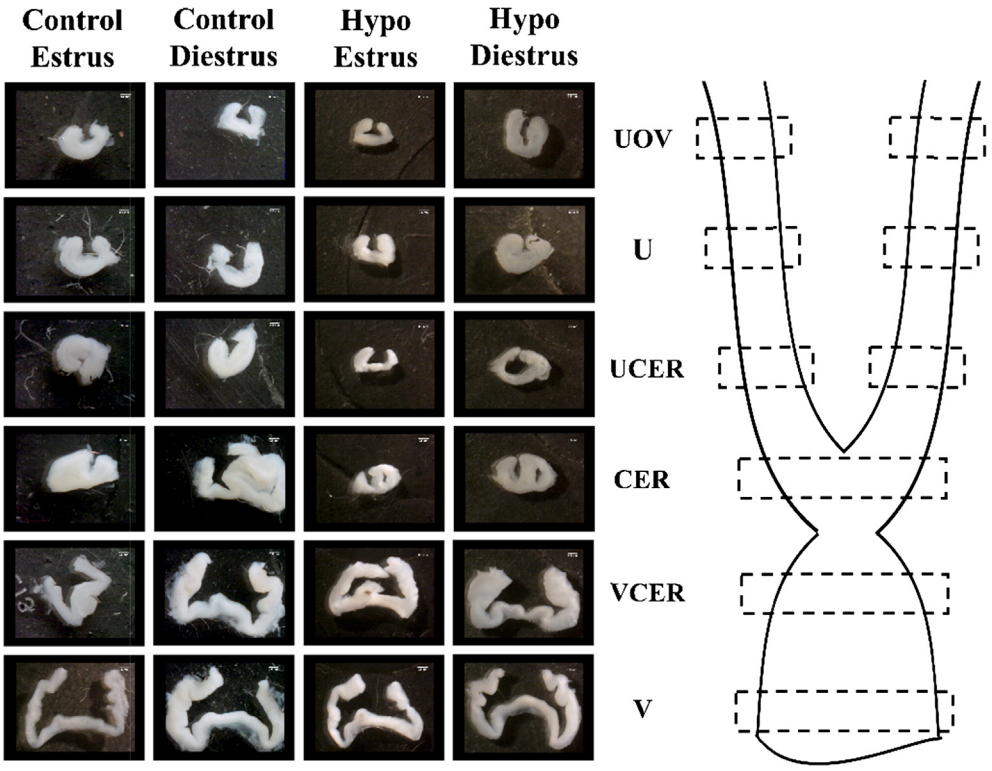

Fig. 1. Representative images of regional opening angles throughout female murine reproductive system. A 0.5 mm transverse cut was made at each of the indicated regions, followed by a radial cut on the anterior of each ring. After a 30 min period, the opening angle images were recorded. Each column is labeled by experimental group (Control Estrus, Control Diestrus, Hypo-osmotic Estrus, and Hypo-osmotic Diestrus). The regions are denoted: UOV (uteri near ovary), U (mid-uteri), UCER (uteri near mid-cervix), CER (mid-cervix), VCER (vaginal cervix), and V (vagina).

specimens at estrus in the control (normo-osmotically loaded) group were fixed in 10% formalin and embedded in paraffin. Sections (4 microns thick) were cut circumferentially followed by deparaffinization and rehydration. For histological analysis, sections were stained with Masson's Trichrome (MTC) and Hart's Elastin stain detecting smooth muscle, collagen, and elastin, respectively. Picrosirius Red (PSR) staining was performed for histological analysis of smaller and larger diameter collagen. For immunohistochemical analysis for area fractions of collagen type III to I, antigen retrieval was performed by rodent decloaker in Nxgen Decloaking chamber (Biocare, Pacheco, CA, USA) at 121 °C for 15 min with pressure (pH = 6.0). The sections were blocked for 5 min in hydrogen peroxide to eliminate endogenous peroxidase activity and nonspecific staining, followed by avidin and biotin blocking. Endogenous mouse IgG was blocked with Rodent BlockM (Biocare, Pacheco, CA, USA) for 30 min. The sections were incubated for 45 min with primary antibodies: rabbit anti-collagen I (1:200; Abcam, Cambridge, MA, USA, ab34710, Lot no. GR321795-4) and rabbit anti-collagen III (1:200; Abcam, Cambridge, MA, USA, ab7778, Lot no. GR3208254-4). Primary antibodies were detected with Rabbit-on-Rodent AP-Polymer (Biocare, Pacheco, CA, USA) with incubation for 45 min. Next, the tissue was incubated in 3,3′-diaminobenzidine substrate for 5 min for color development. Counterstaining with hematoxylin was performed to visualize localization of the collagen types within the tissue.

All images were obtained using an Olympus BX51 microscope and DP-27 camera (Olympus, Tokyo). Samples stained with PSR were imaged with polarized dark field microscopy, and analyzed using a custom MATLAB (Mathworks, Natwick, MA) code to quantify the area fraction of different sized collagen fibers by calculating the number of pixels of each color to quantify the ratio of smaller to larger diameter collagen fibers. MTC, Hart's Elastin, collagen I and collagen III stained images were analyzed using ImageJ (ImageJ, U.S. National Institutes of Health, Bethesda, ME, USA) Color Deconvolution plugin to isolate specific colors based on pixel values (Ruifrok and Johnston, 2001). The GNU Image Manipulation Program (GIMP) was then used to calculate area fractions of each constituent by determining the ratio of stained constituent pixels to total pixels. All quantification was performed on 4× images displaying the full tissue short-axis cross-section.

2.2. Immunoblotting

Reproductive tract tissues (n = 8) were dissected into sections and homogenized in RIPA buffer (ThermoFisher Scientific, Waltham, MA, USA) containing protease and phosphatase inhibitors. Protein concentration was determined by BCA (ThermoFisher Scientific, Waltham, MA, USA) method. Collagen I (n = 3) was resolved by 10% sodium dodecyl sulfate (SDS) gel electrophoresis while collagen III (n = 5) was resolved under 8% non-denaturing conditions with 70 μg of total protein loaded per well. For a standard, 20 μg of human collagen III (Millipore Sigma, Burlington, MA, USA) was used. The proteins were then transferred onto nitrocellulose membranes for 1 h 45 min followed by blocking in LICOR® Odyssey buffer (Lincoln, NE, USA) for 1 h at room temperature. The membranes were incubated in the following primary antibodies overnight at 4 °C: anti-collagen I (1:1000; Abcam, Cambridge, MA, USA, ab34710, Lot no.GR321795-4) or III (1:1000; Abcam, Cambridge, MA, USA, ab7778, Lot no. GR3208254-4). For collagen I blots, β-actin expression was used as a loading control (Cell Signaling Technology, Danvers, MA, USA, 3700, ref. date 082018). For native collagen III blots, Ponceau-S staining (Sigma-Aldrich, St. Louis, MO, USA) was used to verify equal loading of protein. Secondary antibodies used were anti-rabbit (1:2000; Cell Signaling Tehcnology, Danvers, MA, USA) and anti-mouse (1:1000; Santa Cruz Biotechnology, Dallas, TX, USA). The membranes were incubated in Pierce™ ECL Substrate (ThermoFisher Scientific, Waltham, MA, USA) and exposed to autoradiography films to visualize the protein bands. The density of the bands were quantified in ImageJ.

2.3. Data analysis

The circumferential thickness of each ring was calculated using a custom MATLAB (MathWorks, Natwick, MA) script (Ferruzzi et al., 2013). After utilizing ImageJ to find the circumference of each ring, a MATLAB program was written to approximate the volume of each ring using the equation $V = 0.5\pi\left[\left(\frac{D}{2}\right)^2 - \left(\frac{D-2H}{2}\right)^2\right]$ where 0.5 represents the width of the ring in millimeters, D is the outer diameter of the ring in millimeters, which is found by dividing the circumference by pi, and H is the calculated thickness in millimeters. Like the opening angle measurements, the thickness and volume calculations of the rings of the left and right upper uterus near the ovary, left and right mid-uterus, and left and right uteri near the mid-cervix were averaged at each of these locations.

2.4. Statistical analysis

A 3-way ANOVA (estrous cycle, region, hypo-osmotic loading) was used to evaluate changes in opening angle, thickness, and volume in R (*R Foundation for Statistical Computing*). To evaluate regional differences in tissue composition, 1-way ANOVAs were performed for each assay of interest: (1) constituent area fractions obtained from standard histology, (2) ratio of smaller to larger diameter collagen fibers obtained from PSR stained slides, (3) collagen III to I ratio obtained from immunohistochemistry, (4) collagen I content obtained from immunoblotting, and (5) collagen III content obtained from immunoblotting. When appropriate, post-hoc t-tests with Bonferroni corrections were performed.

3. Results

3.1. Opening angle

Opening angle results indicated significant differences ($p < 0.05$) with respect to region and loading; however, the effect of estrous cycle was not found to be significant, nor any of the interactions (Fig. 2). Therefore, to evaluate our hypothesis that regional differences in opening angles are present, post-hoc t-tests with Bonferroni-correction ($p < 0.05/5 = 0.01$) wherein 5 pairwise comparisons were performed within each group (Fig. 2). In all cases, an increasing trend in opening angle was observed in regions increasing distally from the UOV. The vagina exhibited the largest opening angle under each condition except for the normo-osmotic loaded, diestrus group. To investigate our hypothesis that hypo-osmotic loading significantly changes the opening angle, post-hoc t-tests were performed to examine differences in opening angles before and after hypo-osmotic loading. Samples in diestrus exhibited significantly smaller opening angles when subjected to hypo-osmotic loading (Fig. 2A, C). No changes in opening angles were observed in normo-osmotic loaded estrus samples relative to hypo-osmotic loaded samples (Fig. 2B, D).

3.2. Thickness

The 3-way ANOVA identified significant differences ($p < 0.05$) with respect to region (Fig. 3). The effects of estrous cycle and hypo-osmotic loading, however, were not found to be significant, nor any of the interactions. Hence, post-hoc t-tests with Bonferroni-corrections were utilized to examine regional

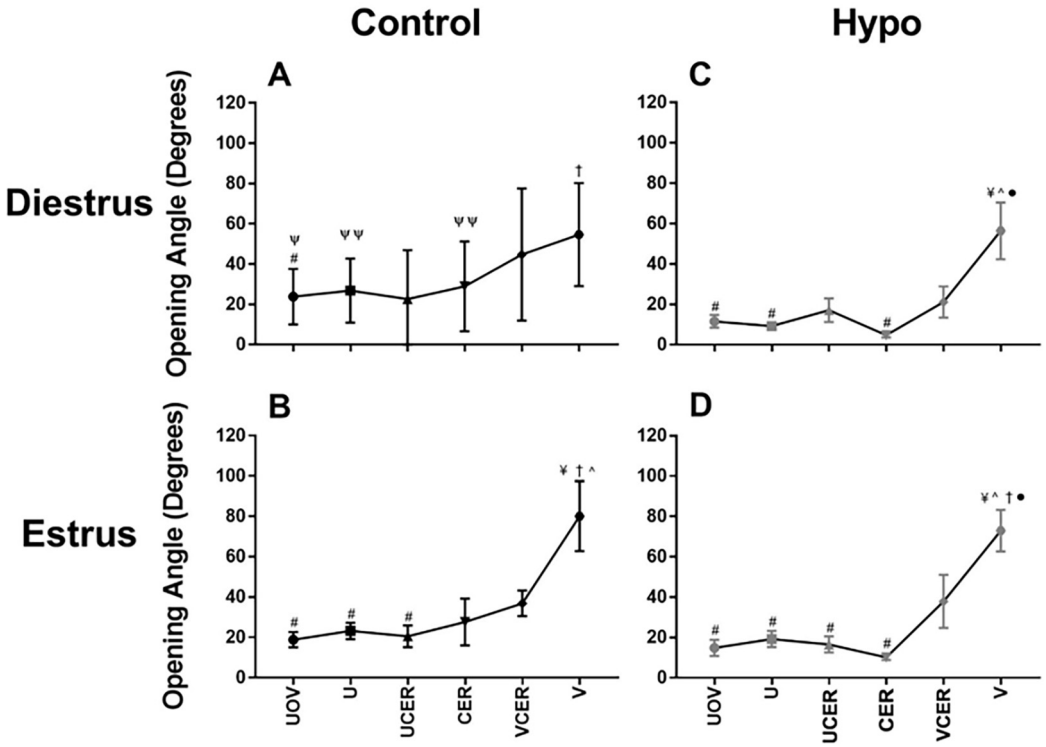

Fig. 2. Diestrus (A, C) and estrus (B, D) opening angles vary along the length of the murine female reproductive system and with hypo-osmotic loading (C, D). Control (normo-osmotically loaded) angles shown in black (A, B) and hypo-osmotically loaded angles in gray (C, D). Ψ indicates statistical significance ($p < 0.01$) with respect to hypo-osmotic loading ($p < 0.05$). †, ¥, ^, •, and # indicate regional significance with respect to UOV, U, UCER, CER, and V, respectively. All data is presented as mean +/− SEM.

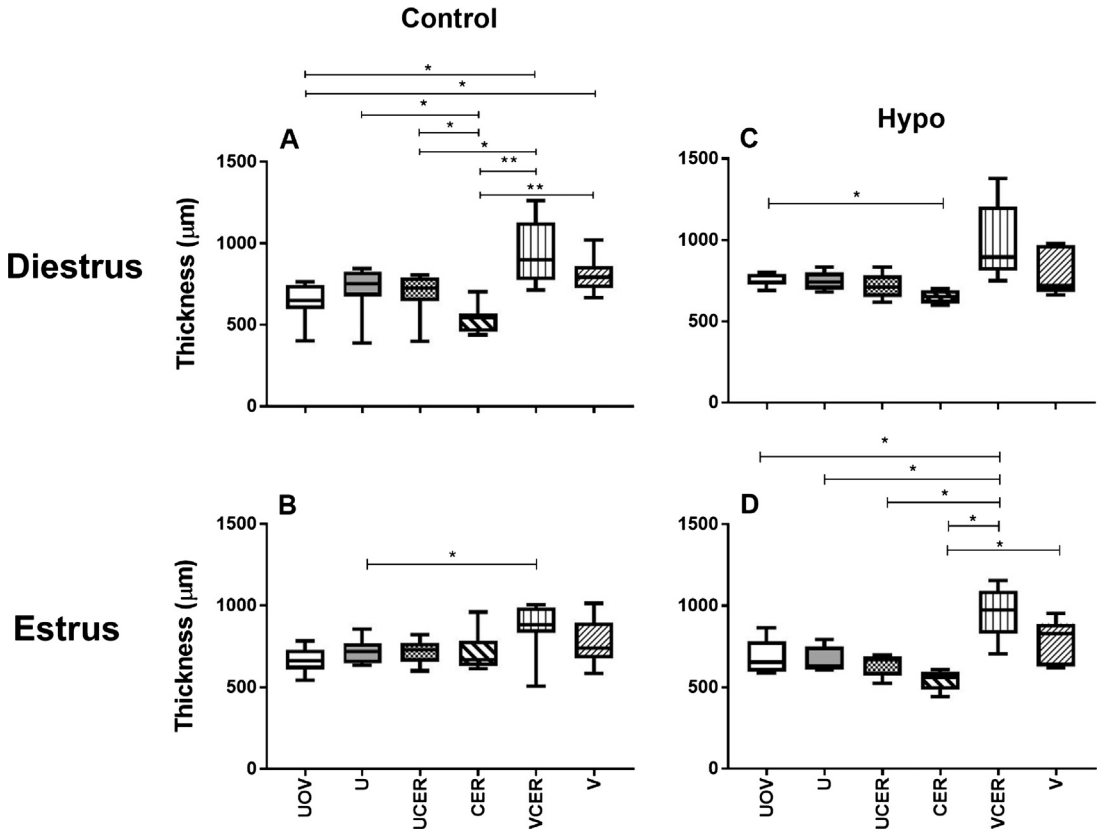

Fig. 3. Thickness values for control (normo-osmotic) (A, B) and hypo-osmotic (C, D) loading throughout the murine female reproductive system at diestrus (A, C) and estrus (B, D). Significant regional differences are indicated by *$p < 0.01$, **$p < 0.001$. Data is presented as the interquartile range with median and upper and lower extremities denoted.

differences ($p < 0.05/5 = 0.01$) wherein 5 pairwise comparisons were performed within each group (Fig. 3).

3.3. Volume

Volume results indicated significant differences ($p < 0.05$) with respect to estrous cycle and region, however the effect of hypo-osmotic loading was not found to be significant, nor any of the interactions (Fig. 4). To test our hypothesis that estrous cycle will induce significant changes in volume, post-hoc t-tests were performed to examine differences in volume at each region in estrus and diestrus. A significant increase ($p < 0.04$) in control VCER sample volume was observed in diestrus, while a significant increase was also observed in hypo-osmotically loaded UOV ($p < 0.03$) and CER ($p < 0.04$) in diestrus. Further, for regional differences in volume, post-hoc t-tests with Bonferroni-correction ($p < 0.05/5 = 0.01$) wherein 5 pairwise comparisons were performed within each group (Fig. 4). Normo-osmotically loaded samples in both estrus and diestrus exhibited significantly larger volumes in the vagina with respect to all regions (Fig. 4A, B).

3.4. Histology, immunohistochemistry, and immunoblotting

The 1-way ANOVA did not identify statistically significant differences in smooth muscle, collagen, and elastin area fraction with regional location (Fig. 5). Statistical analysis revealed significant differences with respect to regional location at estrus in smaller ($p < 0.01$) and larger ($p < 0.001$) diameter collagen area fraction, and smaller to larger diameter ratio ($p < 0.001$) from PSR. The ratio of smaller to larger diameter collagen was significantly greater in the V with respect to all regions (Fig. 5Y). Immunohistochemical analysis with a 1-way ANOVA resulted in no significant difference in collagen III to I ratio between regions (Fig. 5Z). Regional differences in band intensity from immunoblotting for collagen I and III content at estrus were not detected with a 1-way ANOVA (Fig. 6).

4. Discussion

In this study, the effect of estrous cycle, regional variation, and hypo-osmotic loading on residual strain were quantified in the non-pregnant murine female reproductive system. Despite observed changes in collagen composition throughout the estrous cycle (Wood et al., 2007), no significant differences in the opening angle were identified in this study with estrous cycle (Fig. 3). Collagen turnover during the estrous cycle, however, may be constrained to the epithelium, as matrix metalloproteinases (MMPs), collagen degrading molecules, are localized to the epithelium in the murine uterus (Lombardi et al., 2018). Since the stroma is primarily responsible for load-bearing, collagen turnover localized to

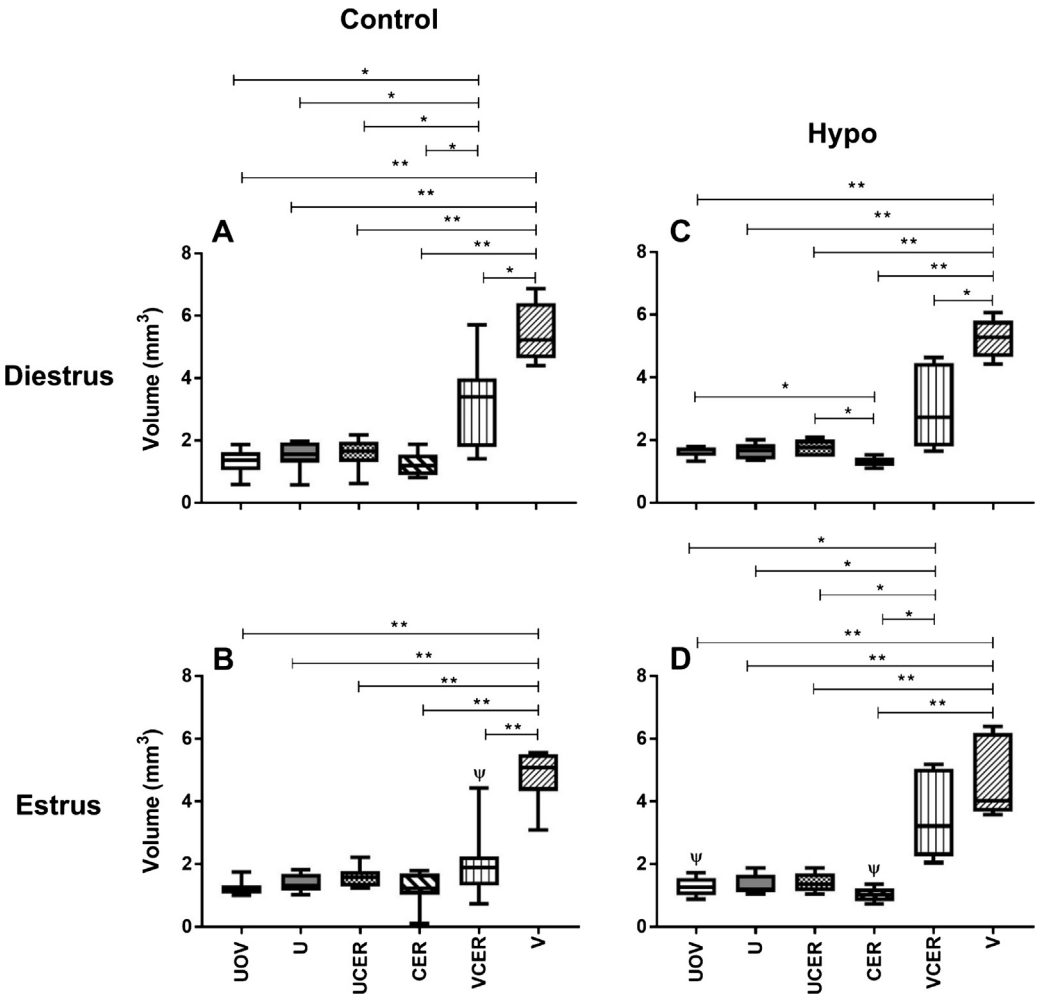

Fig. 4. Control (normo-osmotic) (A, B) and hypo-osmotically (C, D) loaded volumes throughout the murine female reproductive system at diestrus (A, C) and estrus (B, D). Ψ indicates significance ($p < 0.05$) with respect to cycle. Significant regional differences are indicated by *$p < 0.01$, **$p < 0.001$. Data is presented as the interquartile range with median and upper and lower extremities denoted.

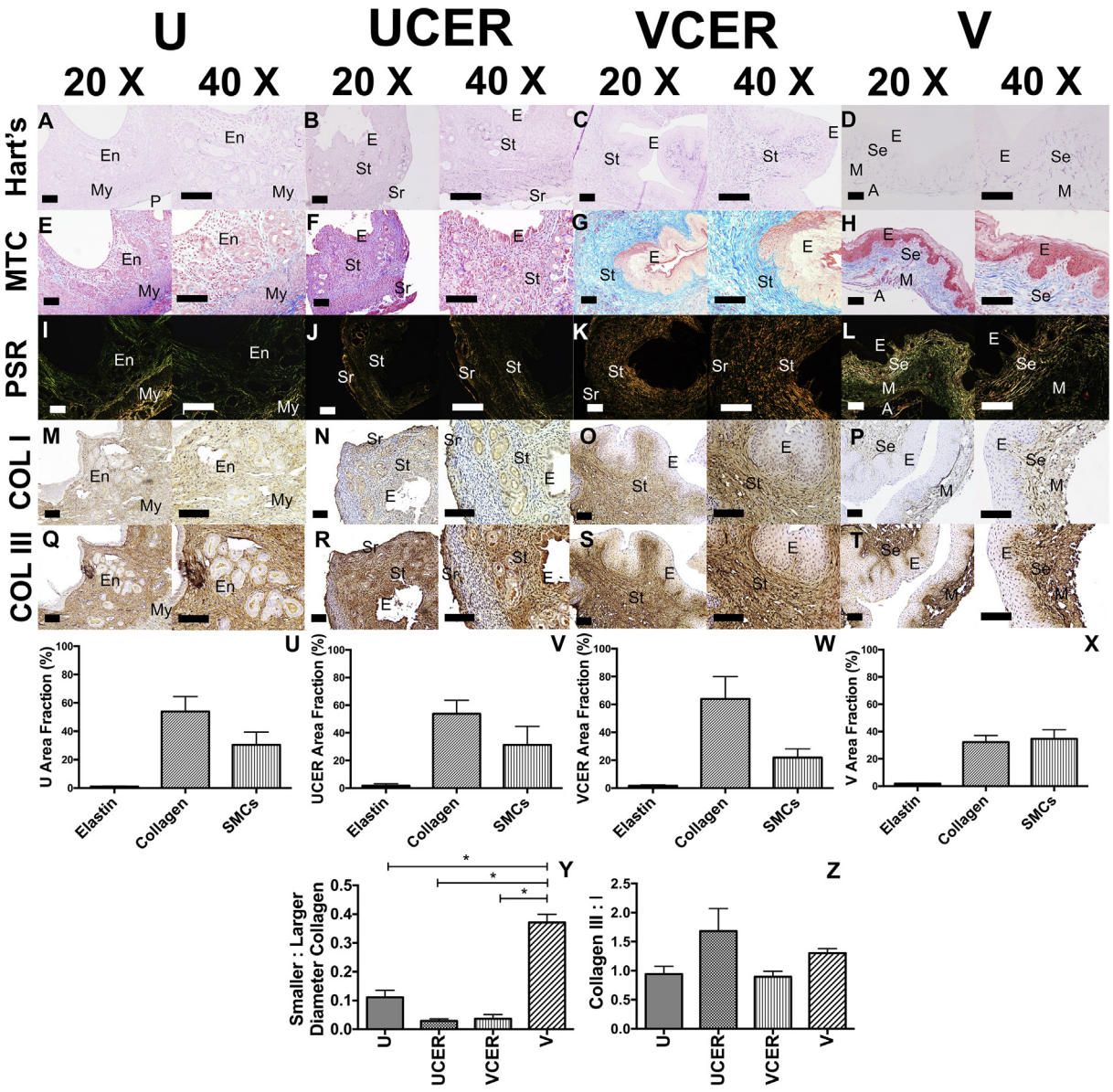

Fig. 5. Circumferential sections of the U (A, E, I, M, Q), UCER (B, F, J, N,R), VCER (C, G, K,O,S), and V (D, H, L,P,T). Histological analysis was performed with Hart's Elastin stain (A-D), Masson's Trichrome (MTC) (E–H), and Picrosirius Red (PSR) (I-L). immunohistochemical analysis was performed for collagen I (COL I) (M-P) and III (COL III) (Q–T). Images displayed acquired at 20× and 40× magnification. Layers of the wall are denoted: En (endometrium), My (myometrium), P (perimetrium), E (epithelium), St (stroma), Sr (serosa), Se (subepithelium), M (muscularis), and A (adventitia). Elastin, collagen, and smooth muscle cell (SMC) area fractions are displayed for each region (U-X). Smaller to larger diameter collagen ratio (Y) and collagen III to I ratio (Z) are shown for each region. Statistical significance is indicated by *$p < 0.005$. Data is reported as mean +/− SEM. Scale bar = 100 μm.

the non-load bearing epithelium may explain the lack of significant differences in residual strain despite altered collagen content. Supporting this, estrous cycle demonstrated no significant changes in material and structural properties in the rat vagina (Moalli et al., 2005) or murine cervix (unpublished pilot study, n = 6).

Estrous cycle, however, significantly affected tissue volume (Fig. 4). Specifically, in normo-osmotic loaded samples, the portion of the cervix closest to the vagina was significantly larger in estrus compared to diestrus; however, hypo-osmotically loaded cervices and uteri near the cervices demonstrated larger volumes in diestrus. The increase in volume may result from alterations in tissue composition between estrus and diestrus. For example, the ewe cervix displayed a greater collagen composition in estrus compared to diestrus (Rodriguez-Pinon et al., 2015). Further, modest increases in GAG content of the murine cervix at diestrus (Akgul et al., 2012b) may contribute to the increase in volume in the hypo-osmotic group as GAGs are water sequestering molecules. Future work is necessary, however, to fully elucidate local changes in tissue microstructure and mechanical function in the murine reproductive system in response to fluctuations in steroid hormones.

Opening angle increased along the length of the reproductive tract (Fig. 2), which may be attributed to differences in tissue microstructure. The vagina demonstrated a larger opening angle and ratio of smaller to larger diameter collagen fibers (PSR analysis) indicating fiber diameter may affect the opening angle. In addition, collagen content is greater in the murine vagina and cervix compared to the uterus (Zhao et al., 2000). Similarly, opening angle and collagen mass fraction increase distally along the length of the aorta (Rachev et al., 2013). The rat esophagus also displayed a positive correlation between collagen content and opening angle (Fan et al., 2005). Prior work implicates that elastin (Greenwald et al.,

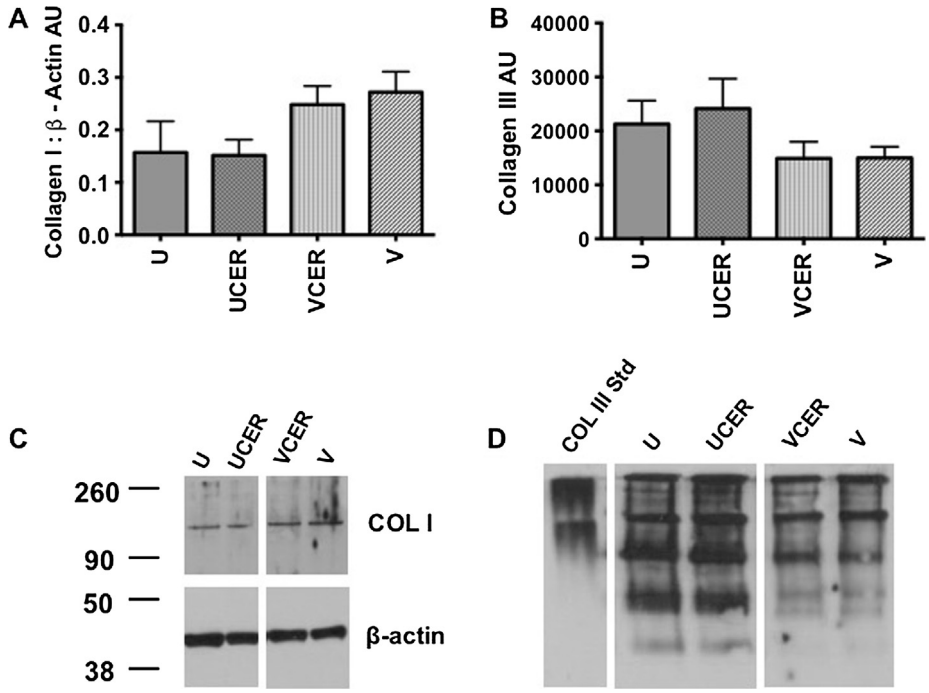

Fig. 6. Immunoblotting for collagen I and III along the female reproductive system. Band intensity across regions for collagen I (A) and III (B) are displayed along with a representative blot (C, D), respectively. Corresponding representative blots display proteins on the same gel of the regions of interest for quantification. Data is reported as mean +/− SEM.

1997) and GAGs (Guo et al., 2007; Sorrentino et al., 2015b; Azeloglu et al., 2008) significantly contribute to residual strain in addition to collagen fibers. No significant differences in elastin area fraction, however, were identified along the length of the reproductive system, thus suggesting collagen fibers may dominate the regional differences observed in this study.

Hypo-osmotic loaded uteri, cervices, and uteri near the ovaries in diestrus exhibited significantly smaller opening angles compared to normo-osmotic loading. A similar trend is reported in the murine carotid artery (Sorrentino et al., 2015a), wherein nonuniform distribution of GAGs may impart this mechanism (as opposed to increased opening angle with hypo-osmotic loading with a uniform distribution) (Guo et al., 2007). In the murine cervix, GAGs are predominantly located within the stroma and epithelial layer and are stabilized by proteoglycans in the stroma (Mahendroo, 2012). Thus, a nonuniform distribution of GAGs and subsequent interactions with proteoglycans may contribute to the decreased OA with hypo-osmotic loading at diestrus. Hypo-osmotic loading, however, did not induce significant changes in opening angles at estrus. Hypo-osmotic loading is thought to increase sequestering of water by hydrophilic GAGs. Thus, the decreased GAG composition at estrus may, in part, explain the lack of significant differences (Akgul et al., 2012b). Similarly, tissue volume and thickness were not significantly altered by hypo-osmotic loading. This result contrasts with increased thickness and volume observed in the murine aorta subjected to hypo-osmotic loading (Guo et al., 2007). Differences arising from distribution of GAG type and interactions with collagen (Greenwald et al., 1997) may affect water sequestration by GAGs. The aorta mainly contains chondroitin sulfate (52% of total GAGs) (Theocharis et al., 1999); contrastingly, hyaluronic acid accounts for 51% of the total GAGs in the non-pregnant murine cervix (Akgul et al., 2012a).

Although not a substitute for studies in human tissues, murine models are widely utilized to investigate the biomechanics of the reproductive system c.f., (Rahn et al., 2008; Robison et al., 2017; Yoshida et al., 2014; Mondragon et al., 2013). Albeit anatomical differences, rodent model's gross connective vaginal tissue anatomy is reported to be similar to humans (Moalli et al., 2005). As for the cervix, despite differences in the non-load bearing epithelium, cervical remodeling processes are comparable to humans (Mahendroo, 2012). Therefore, this animal model serves as a useful tool to assess relationships between the structure and function of the reproductive tissues, including the role of residual strain.

In closing, current computational models do not account for residual strain and report large gradients in transmural stress. This study quantifies residual strain for the potential future incorporation of residual stress into constitutive modeling to describe and predict pelvic floor dynamics. The regional differences observed indicate a significant change in the zero-stress state of each tissue. Such models may aid in the development of constitutive models with predictive capabilities in the treatment and prevention of clinical issues such as premature cervical remodeling and pelvic organ prolapse. Ultimately, the study suggests that incorporation of residual strain into constitutive formulations may aid in evaluations of mechanohomeostasis and mechano-mediated remodeling of the pelvic floor.

Conflict of interest statement

The authors certify that they have NO affiliations with or involvement in any organization or entity with any financial interest (such as honoraria; educational grants; participation in speakers' bureaus; membership, employment, consultancies, stock ownership, or other equity interest; and expert testimony or patent-licensing arrangements), or non-financial interest (such as personal or professional relationships, affiliations, knowledge or beliefs) in the subject matter or materials discussed in this manuscript.

Acknowledgments

We would like to acknowledge Akinjide Akintunde and Cassandra Conway for assistance.

Funding

Tulane Newcomb College Institute (NCI) Faculty Grant (KSM).

References

Abramowitch, S.D., Feola, A., Jallah, Z., Moalli, P.A., 2009. Tissue mechanics, animal models, and pelvic organ prolapse: a review. Eur. J. Obstet. Gynecol. Reprod. Biol. 144 (Suppl 1), S146–S158.

Akgul, Y., Holt, R., Mummert, M., Word, A., Mahendroo, M., 2012. Dynamic changes in cervical glycosaminoglycan composition during normal pregnancy and preterm birth. Endocrinology 153, 3493–3503.

Amin, M., Le, V.P., Wagenseil, J.E., 2012. Mechanical testing of mouse carotid arteries: from newborn to adult. J. Vis. Exp.

Azeloglu, E.U., Albro, M.B., Thimmappa, V.A., Ateshian, G.A., Costa, K.D., 2008. Heterogeneous transmural proteoglycan distribution provides a mechanism for regulating residual stresses in the aorta. Am. J. Physiol.-Heart Circul. Physiol. 294, H1197–H1205.

Barnum, C.E., Fey, J.L., Weiss, S.N., Barila, G., Brown, A.G., Connizzo, B.K., Shetye, S.S., Elovitz, M.A., Soslowsky, L.J., 2017. Tensile mechanical properties and dynamic collagen fiber re-alignment of the murine cervix are dramatically altered throughout pregnancy. J. Biomech. Eng. 139.

Byers, S.L., Wiles, M.V., Dunn, S.L., Taft, R.A., 2012. Mouse estrous cycle identification tool and images. PLoS ONE 7, e35538.

Cardamone, L., Valentin, A., Eberth, J.F., Humphrey, J.D., 2009. Origin of axial prestretch and residual stress in arteries. Biomech. Model Mechanobiol. 8, 431–446.

Chuong, C.J., Fung, Y.C., 1986. On residual stresses in arteries. J. Biomech. Eng. 108, 189–192.

Elovitz, M.A., Mrinalini, C., 2004. Animal models of preterm birth. Trends Endocrinol. Metab. 15, 479–487.

Fan, Y.H., Zhao, J.B., Liao, D.H., Gregersen, H., 2005. The effect of digestion of collagen and elastin on histomorphometry and the zero-stress state in rat esophagus. Dig. Dis. Sci. 50, 1497–1505.

Ferruzzi, J., Bersi, M., Humphrey, J., 2013. Biomechanical phenotyping of central arteries in health and disease: advantages of and methods for murine models. Ann. Biomed. Eng. 41, 1311–1330.

Fung, Y.C., 1991. What are the residual stresses doing in our blood vessels? Ann. Biomed. Eng. 19, 237–249.

Greenwald, S.E., Moore, J.E., Rachev, A., Kane, T.P.C., Meister, J.J., 1997. Experimental investigation of the distribution of residual strains in the artery wall. J. Biomech. Eng.-Trans. ASME 119, 438–444.

Guo, X., Lanir, Y., Kassab, G.S., 2007. Effect of osmolarity on the zero-stress state and mechanical properties of aorta. Am. J. Physiol. Heart Circ. Physiol. 293, H2328–H2334.

Haghighipour, N., Tafazzoli-Shadpour, M., Avolio, A., 2010. Residual stress distribution in a lamellar model of the arterial wall. J. Med. Eng. Technol. 34, 422–428.

Han, H.C., Fung, Y.C., 1996. Direct measurement of transverse residual strains in aorta. Am. J. Physiol. 270, H750–H759.

Humphrey, J.D., 2002. Cardiovascular Solid Mechanics: Cells, Tissues, and Organs. Springer, New York.

Liao, D., Hee, L., Sandager, P., Uldbjerg, N., Gregersen, H., 2014. Identification of biomechanical properties in vivo in human uterine cervix. J. Mech. Behav. Biomed. Mater. 39, 27–37.

Lien, K.C., Mooney, B., DeLancey, J.O.L., Ashton-Miller, J.A., 2004. Levator ani muscle stretch induced by simulated vaginal birth. Obstet. Gynecol. 103, 31–40.

Lombardi, A., Makieva, S., Rinaldi, S.F., Arcuri, F., Petraglia, F., Norman, J.E., 2018. Expression of matrix metalloproteinases in the mouse uterus and human myometrium during pregnancy, labor, and preterm labor. Reprod. Sci. 25, 938–949.

Mahendroo, M., 2012. Cervical remodeling in term and preterm birth: insights from an animal model. Reproduction 143, 429–438.

Moalli, P.A., Howden, N.S., Lowder, J.L., Navarro, J., Debes, K.M., Abramowitch, S.D., Woo, S.L., 2005. A rat model to study the structural properties of the vagina and its supportive tissues. Am. J. Obstet. Gynecol. 192, 80–88.

Mondragon, E., Yoshida, K., Myers, K., 2013. Characterizing the biomechanical and biochemical properties of mouse uterine tissue. Columbia Undergraduate Sci. J. 7, 10–17.

Myers, K.M., Socrate, S., Paskaleva, A., House, M., 2010. A study of the anisotropy and tension/compression behavior of human cervical tissue. J. Biomech. Eng. 132, 021003.

Perry, K., Haresign, W., Wathes, D.C., Pitsillides, A.A., Khalid, M., 2012. Cervical expression of hyaluronan synthases varies with the stage of the estrous cycle in the ewe. Theriogenology 77, 1100–1110.

Rachev, A., Greenwald, S., Shazly, T., 2013. Are geometrical and structural variations along the length of the aorta governed by a principle of "optimal mechanical operation"? J. Biomech. Eng.-Trans. ASME 135, 9.

Rahn, D.D., Ruff, M.D., Brown, S.A., Tibbals, H.F., Word, R.A., 2008. Biomechanical properties of the vaginal wall: effect of pregnancy, elastic fiber deficiency, and pelvic organ prolapse. Am. J. Obstet. Gynecol. 198 (590), e1–e6.

Robison, K.M., Conway, C.K., Desrosiers, L., Knoepp, L.R., Miller, K.S., 2017. Biaxial mechanical assessment of the murine vaginal wall using extension-inflation testing. J. Biomech. Eng. 139.

Rodriguez-Pinon, M., Tasende, C., Casuriaga, D., Bielli, A., Genovese, P., Garofalo, E.G., 2015. Collagen and matrix metalloproteinase-2 and -9 in the ewe cervix during the estrous cycle. Theriogenology 84, 818–826.

Ruifrok, A.C., Johnston, D.A., 2001. Quantification of histochemical staining by color deconvolution. Anal. Quant. Cytol. Histol. 23, 291–299.

Sorrentino, T.A., Fourman, L., Ferruzzi, J., Miller, K.S., Humphrey, J.D., Roccabianca, S., 2015a. Local versus global mechanical effects of intramural swelling in carotid arteries. J. Biomech. Eng.-Trans. ASME 137, 8.

Sorrentino, T.A., Fourman, L., Ferruzzi, J., Miller, K.S., Humphrey, J.D., Roccabianca, S., 2015b. Local versus global mechanical effects of intramural swelling in carotid arteries. J. Biomech. Eng. 137.

Taber, L.A., Humphrey, J.D., 2001. Stress-modulated growth, residual stress, and vascular heterogeneity. J. Biomech. Eng. 123, 528–535.

Taghizadeh, H., Tafazzoli-Shadpour, M., Shadmehr, M.B., 2015. Analysis of arterial wall remodeling in hypertension based on lamellar modeling. J. Am. Soc. Hypertens 9, 735–744.

Takamizawa, K., Hayashi, K., 1987. Strain energy density function and uniform strain hypothesis for arterial mechanics. J. Biomech. 20, 7–17.

Takamizawa, K., Hayashi, K., 1988. Uniform strain hypothesis and thin-walled theory in arterial mechanics. Biorheology 25, 555–565.

Theocharis, A.D., Tsolakis, I., Tsegenidis, T., Karamanos, N.K., 1999. Human abdominal aortic aneurysm is closely associated with compositional and specific structural modifications at the glycosaminoglycan level. Atherosclerosis 145, 359–368.

Westervelt, A.R., Myers, K.M., 2017. Computer modeling tools to understand the causes of preterm birth. Semin. Perinatol. 41, 485–492.

Wood, G.A., Fata, J.E., Watson, K.L.M., Khokha, R., 2007. Circulating hormones and estrous stage predict cellular and stromal remodeling in murine uterus. Reproduction 133, 1035–1044.

Yang, Z., Hayes, J., Krishnamurty, S., Grosse, I.R., 2016. 3D finite element modeling of pelvic organ prolapse. Comput. Meth. Biomech. Biomed. Eng. 19, 1772–1784.

Yoshida, K., Jiang, H., Kim, M., Vink, J., Cremers, S., Paik, D., Wapner, R., Mahendroo, M., Myers, K., 2014. Quantitative evaluation of collagen crosslinks and corresponding tensile mechanical properties in mouse cervical tissue during normal pregnancy. PLoS ONE 9, e112391.

Zhao, L., Samuel, C.S., Tregear, G.W., Beck, F., Wintour, E.M., 2000. Collagen studies in late pregnant relaxin null mice. Biol. Reprod. 63, 697–703.